DISCONTINUOUS GALERKIN METHODS FOR SOLVING THE ACOUSTIC WAVE EQUATION

Gabriel A. Castromán and Fabio I. Zyserman

CONICET, Departamento de Geofísica Aplicada, Fac. de Cs. Astronómicas y Geofísicas, Universidad Nacional de La Plata, Paseo del Bosque s/n, 1900 - La Plata, Argentina
gcastroman@fcaglp.unlp.edu.ar, zyserman@fcaglp.unlp.edu.ar

Abstract. In this work we develop a numerical simulator for the propagation of elastic waves by solving the one-dimensional acoustic wave equation with Absorbing Boundary Conditions (ABC's) on the computational boundaries using Discontinuous Galerkin Finite Element Methods (DGFEM). The DGFEM allows us to easily simulate the presence of a fracture in the elastic medium by means of a linear-slip model. We analize the behaviour of our algorithm by comparing its results against analytic solutions. Furthermore, we show the frequency-dependent effect on the propagation produced by the fracture as appears in previous works. Finally, we present an analysis of the numerical parameters of the method.

1 INTRODUCTION

The waves that propagate into the Earth's interior give us information about its mechanical and physical properties. The study and analysis of these waves allows us to infer the different structures in the Earth's subsurface, as well as the type of rocks and the presence of fluids. It is therefore an interesting topic for both the petroleum industry and academic studies.

Numerical simulation is a very valuable tool for this purpose. The numerical resolution of the wave equation enables us to predict the behaviour of the waves traveling through very complex heterogeneus media, as the Earth's interior. Is for this reason that we look for numerical methods that can solve this problems with high accuracy and stability.

In this work we develop and implement Discontinuous Galerkin Finite Element Methods (DGFEM) for the resolution of the one-dimensional acoustic wave equation with Absorbing Boundary Conditions (ABC's) on the boundaries of the computational domain. Besides of having a high order of accuracy, the choice of this method lies in its capability to simulate in a natural way the presence of a fracture in the elastic medium. Fractures are a very important feature in the characterization of the subsurface for a wide range of scales, from faults to microcracks; unconventional reservoirs in the petroleum industry are strongly related to fractured media. The presence of a single natural fracture is simulated by means of a linear slip model (Schoenberg, 1980). The advantage of using this method over the equivalent medium theory is that it requieres fewer assumptions and can handle more complex geometries for the fracture. Different applications of DGFEM in engineering problems such as radiative transfer and shallow water flows can be seen in Álvarez Tagliabue and Marino (2007) and Tassi and Vionnet (2003) respectively.

2 ELASTIC WAVE EQUATION

To simulate seismic wave propagation (i.e. the propagation of waves into the Earth's interior) we need to solve the wave equation for the displacement field $\vec{u}(\vec{x}, t)$ as a function of space and time in an elastic medium. This equation can be derived from the equation of motion for a particle of the medium and the theory of linear elasticity, wich establish the relationship between strain (deformation) and stress, through the Hooke's law (Udías, 1999). For an elastic and isotropic medium in the one-dimensional case, this equation reduces to

$$\rho(x)\ddot{u}(x, t) - \left\{ [2\mu(x) + \lambda(x)] \, u'(x, t) \right\}' = f(x, t), \tag{1}$$

where λ and μ are the Lamé's coefficients, ρ is the density of the medium and f is the volumetric external force (source). The physical properties of the medium are functions of space, while displacements and the external source are functions of both space and time. Dot notation is used for time derivatives and primed notation for spatial derivatives. This equation can be expressed in the space-frequency domain as follows

$$-\omega^2 \rho(x)\hat{u}(x, \omega) - [k(x)\hat{u}'(x, \omega)]' = \hat{f}(x, \omega), \tag{2}$$

where ω is the angular frequency, $k = 2\mu + \lambda$ is the longitudinal modulus and $\hat{u}$, $\hat{f}$ are the Fourier transforms of the displacements and the external source respectively. In order to completely state our problem, we must to establish the boundary conditions for the elastic medium. In this work we use Absorbing Boundary Conditions (ABC's) on the computational boundaries, which

allows the waves travelling out the computational domain $\Omega = [a, b]$ pass the boundaries without reflections. In the one-dimensional case, the equation for ABC's proposed by Gauzellino et al. (2001) in the space-frequency domain leads to the expressions

$$
\begin{aligned}
k(x)\hat{u}(x,\omega) &= i\omega\sqrt{k(x)\rho(x)}\,\hat{u}(x,\omega), \qquad x = a, \qquad \omega > 0, \\
-k(x)\hat{u}(x,\omega) &= i\omega\sqrt{k(x)\rho(x)}\,\hat{u}(x,\omega), \qquad x = b, \qquad \omega > 0.
\end{aligned} \tag{3}
$$

As was mentioned before, one of the reasons of using DGFEM is that allows us to simulate the presence of a single fracture in a natural way, instead of using effective medium theories. For this purpouse, we use a linear slip model proposed by Schoenberg (1980) which represents a fracture in the elastic medium by means of a discontinuity of the displacement. The tension remains constant in the fracture location and is linearly related to the jump of the displacement, or slip, as shown below

$$
[\hat{u}(x_\gamma,\omega)] = -Zk(x_\gamma)\hat{u}'(x_\gamma,\omega), \tag{4}
$$

where x_γ is the fracture location, $[\hat{u}]$ is the jump of the displacement and Z is the normal compliance of the fracture.

3 DISCONTINUOUS GALERKIN FINITE ELEMENT METHOD

The DGFEM is one of the multiple variations of the finite element method. Besides of having the advantages of the continuous methods, allows for the approximate global solution to be discontinuous at the interfaces between elements without introducing spurious numerical oscillations. This is due to the local support of the basis of the finite-dimensional space where we look for the approximate solution; the continuity of the numerical solution is imposed weakly through additional penalty parameters.

Following the proccedure descript in Riviere (2008) consider a partition $\mathcal{E}_h$ of the domain Ω of the form $a = x_0 < x_1 < \cdots < x_N = b$, where the n-th element is defined as $I_n = (x_n, x_{n+1})$ for $n = 0, 1, \cdots, N-1$, being N the number of elements. The size of the n-th element is given by $h_n = x_{n+1} - x_n$. For the finite-dimensional space we consider the space of piecewise discontinuous polynomials of degree r defined as follows

$$
\mathcal{D}_r(\mathcal{E}_h) = \{v(x): \ v(x)|_{I_n} \in \mathbb{P}_r(I_n); \ \forall n = 0, 1, ..., N-1\}, \tag{5}
$$

where $\mathbb{P}_r(I_n)$ is the space of polynomials of degree r in the n-th element. Because of their definition, the functions $v(x)$ can be discontinuous at the nodes x_n. Thus, we can define the jump and the average of the function v as

$$
[v(x_n)] = v(x_n^-) - v(x_n^+), \qquad\qquad \{v(x_n)\} = \frac{v(x_n^-) + v(x_n^+)}{2}, \tag{6}
$$

where $v(x_n^+) = \lim_{\delta\to 0^+} v(x_n+\delta)$ and $v(x_n^-) = \lim_{\delta\to 0^-} v(x_n+\delta)$. The average and jump at the boundaries are $[v(x_0)] = -v(x_0^+)$, $\{v(x_0)\} = v(x_0^+)$, $v[(x_N)] = v(x_N^-)$ and $\{v(x_N)\} = v(x_N^-)$.

Based on this definitions, the weak formulation of the problem is obtained by integrating by parts on each element the space-frequency acoustic wave equation multiplied by an arbitrary trial function $v(x)$ and summing over all elements, with the addition of the boundary condition

terms and the fracture condition. Also, for the stabilization of the problem, two more extra terms are added: a term including the interior penalty parameters and a term which leads to different interior penalty DGFEM's. We define then the bilinear form $a_\epsilon : \mathcal{D}_r(\mathcal{E}_h) \times \mathcal{D}_r(\mathcal{E}_h) \to \mathbb{R}$

$$
\begin{aligned}
a_\epsilon\big(\hat{u}(x), v(x)\big) = &\sum_{n=0}^{N-1} \int_{x_n}^{x_{n+1}} \Big(k(x)\hat{u}'(x)v'(x) - \omega^2 \rho(x)\hat{u}(x)v(x) \Big) dx + \frac{1}{Z}[\hat{u}(x_\gamma)][v(x_\gamma)] \\
&+ \sum_{\substack{n=1 \\ n \neq \gamma}}^{N-1} \Big(\{k(x_n)\hat{u}'(x_n)\}[v(x_n)] + \epsilon\{k(x_n)v'(x_n)\}[\hat{u}(x_n)] + \frac{\sigma_n}{h_n}[v(x_n)][\hat{u}(x_n)] \Big) \\
&+ i\omega\big(k(x_0)\rho(x_0)\big)^{\frac{1}{2}}\hat{u}(x_0)v(x_0) + i\omega\big(k(x_N)\rho(x_N)\big)^{\frac{1}{2}}\hat{u}(x_N)v(x_N)
\end{aligned}
$$
(7)

where σ_n are the interior penalty parameters and ϵ takes the values $\{-1, 0, 1\}$ for the Symmetric, Incomplete and Non-symmetric Interior Penalty Methods respectively (SIPG, IIPG and NIPG). To simplify the notation, the depence of $\hat{u}$ and $\hat{f}$ with the frequency is not explicited. Assumming the existence and uniqueness of the solution $\hat{u}^{DG}(x)$, we can postulate the weak formulation of the problem as follows: find $\hat{u}^{DG}(x) \in \mathcal{D}_r(\mathcal{E}_h)$, that $\forall v(x) \in \mathcal{D}_r(\mathcal{E}_h)$

$$
a_\epsilon\big(\hat{u}^{DG}(x), v(x)\big) = \mathcal{L}\big(v(x)\big),
$$
(8)

where the linear form $\mathcal{L} : \mathcal{D}_r(\mathcal{E}_h) \to \mathbb{R}$ is defined as:

$$
\mathcal{L}\big(v(x)\big) = \int_{x_0}^{x_N} v(x)\hat{f}(x) dx.
$$
(9)

To derive from this weak formulation a linear system that can be solved numerically, we first have to set the local and global basis functions of the spaces $\mathbb{P}_r(I_n)$ and $\mathcal{D}_r(\mathcal{E}_h)$ respectively. The local basis functions $\{\phi_d^n(x)\}$ with $d = 0, 1, \cdots, r$, $n = 0, 1, \cdots, N-1$ are such that $\mathbb{P}_r(I_n) = span\{\phi_0^n(x), \phi_1^n(x), \cdots, \phi_r^n(x)\}$ and are defined as

$$
\phi_d^n(x) = 2^d \left(\frac{x - x_{n+1/2}}{x_{n+1} - x_n} \right)^d,
$$
(10)

where $x_{n+1/2} = x_n + h_n/2$ is the middle point of the interval I_n. The global basis functions $\{\Phi_d^n(x)\}$ are obtained by extending by zero the local basis functions over the entire domain as follows

$$
\Phi_d^n(x) = \begin{cases} \phi_d^n(x) & x \in I_n \\ 0 & x \notin I_n. \end{cases}
$$
(11)

The approximate solution $\hat{u}^{DG}(x), \forall x \in (x_0, x_N)$ is expressed in this basis as:

$$
\hat{u}^{DG}(x) = \sum_{m=0}^{N-1} \sum_{j=0}^{r} \alpha_j^m \Phi_j^m(x),
$$
(12)

where α_j^m, $j = 0, 1, \cdots, r$, $n = 0, 1, \cdots, N - 1$, are the coefficients that characterize the solution in the finite-dimensional space and are the unknowns we are looking for. Replacing the expression of $\hat{u}^{DG}(x)$ into eq. (8), taking into account that this equation must be satisfied $\forall v(x) \in \mathcal{D}_r(\mathcal{E}_h)$ and making use of the properties of the bilinear form a_ϵ, we can derive a linear system $A\vec{\alpha} = \vec{b}$ where

$$\vec{\alpha} = (\alpha_0^0, \alpha_1^0, \cdots, \alpha_r^0, \alpha_0^1, \alpha_1^1, \cdots, \alpha_r^1, \cdots, \alpha_0^{N-1}, \alpha_1^{N-1}, \cdots, \alpha_r^{N-1})^T \tag{13}$$

is a column vector of length $(r+1)N$ containing the unknowns; the right-hand side $\vec{b}$ is a column vector of length $(r+1)N$ with coefficients b_i^n, $i = 0, 1, \cdots, r$, $n = 0, 1, \cdots, N - 1$ disposed as follows:

$$\vec{b} = (b_0^0, b_1^0, \cdots, b_r^0, b_0^1, b_1^1, \cdots, b_r^1, \cdots, b_0^{N-1}, b_1^{N-1}, \cdots, b_r^{N-1})^T; \tag{14}$$

and

$$A = \begin{pmatrix} M_0 & D_1 & 0 & \cdots & 0 \\ E_1 & M_1 & D_2 & \ddots & \vdots \\ 0 & \ddots & \ddots & \ddots & 0 \\ \vdots & \ddots & E_{N-2} & M_{N-2} & D_{N-1} \\ 0 & \cdots & 0 & E_{N-1} & M_{N-1} \end{pmatrix} \tag{15}$$

is a block tridiagonal matrix with M_0, M_n, D_n and E_n, $n = 1, 2, \cdots, N-1$ being local matrices of dimension $(r+1) \times (r+1)$ that can be computed separately because of the local support of the global basis functions. This matrices and the coefficients of the right-hand side for $r = 2$ are explicitely shown in Appendix A.

4 NUMERICAL EXAMPLES

To completely characterize our problem we have to define the source implementation. Many problems in seismic wave propagation require the use of point sources; to simulate a compressional point source in one dimension, we use a derivative of the Dirac Delta distribution $\delta'(x)$ in space and a Ricker wavelet $f_R(t)$ (Ricker, 1940) as the source time function

$$f(x, t) = \delta'(x - x_f) f_R(t), \tag{16}$$

where x_f is the location of the source and $f_R(t)$ has the form

$$f_R(t) = \left[1 - 2\pi^2 f_p^2 (t - dr)^2\right] e^{-\pi^2 f_p^2 (t-dr)^2}, \tag{17}$$

where f_p is the central frequency of the wavelet and dr is the time shift. The source representation in the frequency domain $\hat{f}_R(\omega)$ is given by the Fourier transform of $f_R(t)$:

$$\hat{f}_R(\omega) = \frac{-2}{f_p\sqrt{\pi}} \left(\frac{\omega}{2\pi f_p}\right)^2 e^{-i\omega dr - \left(\frac{\omega}{2\pi f_p}\right)^2}. \tag{18}$$

This expression is used in Appendix A to obtain the explicit form of the right-hand side $\vec{b}$.

4.1 Homogeneus medium

The analytic solution of eq. (1) for an infinite homogeneus medium with the source recently defined is

$$
u(x,t) = \begin{cases} \dfrac{1}{2v_l^2\rho} f_R\left(t + \dfrac{x - x_f}{v_l}\right), & x < x_f, \qquad t > 0; \\[4mm] -\dfrac{1}{2v_l^2\rho} f_R\left(t - \dfrac{x - x_f}{v_l}\right), & x > x_f, \qquad t > 0; \end{cases} \tag{19}
$$

where v_l is the longitudinal velocity of propagation, given by $v_l = \sqrt{k/\rho}$. In the frequency domain the analytic solution has the form

$$
\hat{u}(x,\omega) = \begin{cases} \dfrac{1}{2v_l^2\rho} \hat{f}_R(\omega) e^{i\left(\frac{x - x_f}{v_l}\right)\omega}, & x < x_f; \\[4mm] -\dfrac{1}{2v_l^2\rho} \hat{f}_R(\omega) e^{-i\left(\frac{x - x_f}{v_l}\right)\omega}, & x > x_f. \end{cases} \tag{20}
$$

As a test case, consider an homogeneus medium represented by $\Omega = [0, 1000]m$ with density $\rho = 2500 kg/m^3$ and velocity $v_l = 2200 m/s$. The source, located at $x_f = 100m$, has a central frequency of $f_p = 30Hz$ and a time shift of $dr = 33ms$. The linear system derived in the previous section is solved using a Block Tridiagonal LU Factorization Method (see Appendix B) for a fixed frecuency $\omega_p = 2\pi f_p$. Throughout the present work we will use an uniform mesh with element size h and a constant penalty parameter σ for all the nodes in the domain. The three methods proposed (SIPG, IIPG and NIPG) are tested for linear and quadratic polynomial basis functions (spaces $\mathcal{D}_1(\mathcal{E}_h)$ and $\mathcal{D}_2(\mathcal{E}_h)$ respectively). The approximate solutions $\hat{u}^{DG}(x, \omega_p)$ obtained are compared with the analytic solution $\hat{u}(x, \omega_p)$ and the results are shown below.

Relative errors ($l2$-norm) are listed for the SIPG method in Table 1 and Table 2 for linear and quadratic approximations. Table 3 and Table 4 correspond to the IIPG method. For the NIPG method, errors are presented in Table 5 and Table 6. In all cases, the element size h and the penalty parameter σ take the values $\{8m, 4m, 2m, 1m\}$ and $\{1000, k, 1000k\}$ respectively, where $k = 12.13 \times 10^9$ is the magnitude of the longitudinal modulus here considered.

	$\sigma = 1000$	$\sigma = k$	$\sigma = 1000k$
$h = 8$	9.037×10^{-1}	4.688×10^{0}	7.829×10^{-1}
$h = 4$	3.837×10^{-1}	1.087×10^{2}	3.733×10^{-1}
$h = 2$	1.368×10^{-1}	1.488×10^{2}	1.362×10^{-1}
$h = 1$	5.504×10^{-2}	1.204×10^{2}	5.502×10^{-2}

Table 1: Relative error ($l2$-norm) for the SIPG method with $\mathcal{D}_1(\mathcal{E}_h)$

	$\sigma = 1000$	$\sigma = k$	$\sigma = 1000k$
$h = 8$	5.686×10^{-2}	1.970×10^{-1}	2.042×10^{-2}
$h = 4$	6.594×10^{-3}	1.637×10^{-1}	9.492×10^{-3}
$h = 2$	7.524×10^{-4}	1.469×10^{-1}	2.370×10^{-3}
$h = 1$	9.515×10^{-5}	1.353×10^{-1}	5.929×10^{-4}

Table 2: Relative error ($l2$-norm) for the SIPG method with $\mathcal{D}_2(\mathcal{E}_h)$.

	$\sigma = 1000$	$\sigma = k$	$\sigma = 1000k$
$h = 8$	1.141×10^{1}	1.000×10^{0}	7.814×10^{-1}
$h = 4$	4.347×10^{1}	1.000×10^{0}	3.727×10^{-1}
$h = 2$	1.720×10^{2}	1.000×10^{0}	1.360×10^{-1}
$h = 1$	6.863×10^{2}	1.000×10^{0}	5.502×10^{-2}

Table 3: Relative error ($l2$-norm) for the IIPG method with $\mathcal{D}_1(\mathcal{E}_h)$.

	$\sigma = 1000$	$\sigma = k$	$\sigma = 1000k$
$h = 8$	0.999×10^{0}	1.000×10^{0}	2.164×10^{-2}
$h = 4$	1.000×10^{0}	1.163×10^{0}	8.557×10^{-3}
$h = 2$	1.000×10^{0}	1.036×10^{0}	1.404×10^{-3}
$h = 1$	1.000×10^{0}	1.008×10^{0}	4.309×10^{-4}

Table 4: Relative error ($l2$-norm) for the IIPG method with $\mathcal{D}_2(\mathcal{E}_h)$.

	$\sigma = 1000$	$\sigma = k$	$\sigma = 1000k$
$h = 8$	4.083×10^{0}	1.000×10^{0}	7.785×10^{-1}
$h = 4$	2.704×10^{0}	1.000×10^{0}	3.704×10^{-1}
$h = 2$	4.980×10^{0}	1.000×10^{0}	1.340×10^{-1}
$h = 1$	2.863×10^{0}	1.000×10^{0}	5.312×10^{-2}

Table 5: Relative error ($l2$-norm) for the NIPG method with $\mathcal{D}_1(\mathcal{E}_h)$.

	$\sigma = 1000$	$\sigma = k$	$\sigma = 1000k$
$h = 8$	1.315×10^{0}	9.336×10^{0}	2.225×10^{-2}
$h = 4$	2.165×10^{0}	1.131×10^{0}	7.346×10^{-3}
$h = 2$	2.041×10^{0}	1.023×10^{0}	1.463×10^{-3}
$h = 1$	2.009×10^{0}	1.006×10^{0}	6.288×10^{-4}

Table 6: Relative error ($l2$-norm) for the NIPG method with $\mathcal{D}_2(\mathcal{E}_h)$.

We first analyze the influence of the penalty parameter σ. Comparing the third column ($\sigma = 1000k$) of Table 1 (SIPG), Table 3 (IIPG) and Table 5 (NIPG) we can observe that, for such a large value of the penalty, all the discontinuous methods using $\mathcal{D}_1(\mathcal{E}_h)$ have the same rate of convergence with h. A similar situation occurs with $\mathcal{D}_2(\mathcal{E}_h)$, as is shown in the third column of Tables 2, 4 and 6, with the difference that the rate of the quadratic approximation is larger than the linear one and errors are smaller. For a value of the penalty parameter $\sigma = k$, only the SIPG method with a quadratic approximation (second column of Table 2) shows convergence with h, but errors are larger than the ones in columns $\sigma = 1000$ and $\sigma = 1000k$ of Table 2. For

$\sigma = 1000$, only the SIPG method shows convergence with h, for both the linear and quadratic approximation (first column of Tables 1 and 2 respectively). The rate of convergence of the SIPG method using $\mathcal{D}_2(\mathcal{E}_h)$ with this penalty is greater than the ones obtained with $\sigma = 1000$ and $\sigma = 1000k$, and errors are smaller; but we can assert that in general the DGFEM has a better performance with a large enough penalty parameter.

Comparing the three different methods we can observe that the SIPG method shows convergence with h for both linear and quadratic approximation and all the penalty parameters considered (except for $\sigma = k$ in linear approximation). The IIPG and NIPG methods present large errors for lower penalties, specially for $\sigma = 1000$, where the methods seem to be unstable.

We finish this analysis comparing the linear and quadratic approximations by means of the computational cost of the method, which in this case is controlled by the size of the global matrix A. Using linear basis functions the corresponding size is $2N \times 2N$ and with quadratic basis functions is $3N' \times 3N'$, where N and N' are the number of elements considered for each case. For the SIPG method with a penalty $\sigma = 1000k$ we compare the errors with a mesh spacing $h = 2m$ for the linear approximation and $h = 4m$ for the quadratic approximation. In the first case, the total number of elements is $N = 500$ and then the size of A is 1000×1000. In the second one, the number of elements is $N' = 250$ and then the size of the global matrix is 750×750. We can observe that the error yielded by the linear approximation is greater than the one of the quadratic approximation, even when the size of the global matrix is larger in the former case. Therefore the quadratic approximation has a better precision with lower computational cost. In what follows we will use the quadratic order SIPG method with a large value of penalty ($\sigma = 1000k$).

To obtain an approximate solution in time we have to solve the linear system for a number npf of points in frequency, and once the approximate solution $\hat{u}^{DG}(x, \omega_m)$, $m = 1, 2, \cdots, npf$ is calculated, use an inverse Fourier transform to obtain $u^{DG}(x, t)$. Fig. 1 correspond to different seismic traces, i.e. the variation of the displacement with time for a fixed position x_{rec}. In green we have the linear approximation and in red the quadratic approximation for a mesh spacing of $2m$. The analytic solution $u(x_{rec}, t)$ is shown in blue.
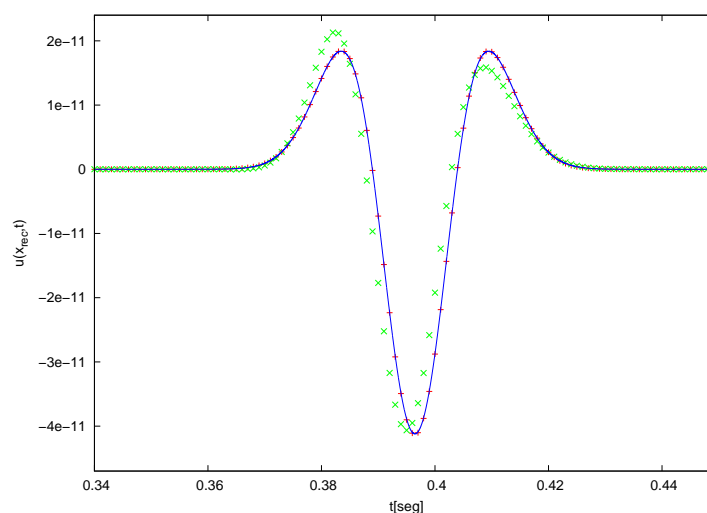

Figure 1: Seismic traces $u^{DG}(x_{rec}, t)$ registered at location $x_r = 900m$ for linear (green) and quadratic (red) approximations, and the analytic solution $u(x_{rec}, t)$ (blue solid line).

4.2 Homogeneus medium with a single fracture

In order to test the implementation of the linear slip model in the DGFEM scheme, we simulate the propagation of seismic waves in an homogeneus medium with the inclusion of a single natural fracture of normal compliance $Z = 2.3m/GPa$ located at $x_\gamma = 1000m$. The homogeneus background has a longitude of $2000m$, a density $\rho = 2000kg/m^3$ and a longitudinal velocity $v_l = 3415m/s$. The source is the same used in the previous subsection and is located at $x_f = 700m$. Fig. 2 shows the seismic trace obtained at the location $x_{r1} = 850m$ and Fig. 3 the one obtained at $x_{r2} = 1200m$ in addition to the analytic solution for an homogeneus medium in the same conditions without the fracture. The mesh spacing used is $h = 2m$.
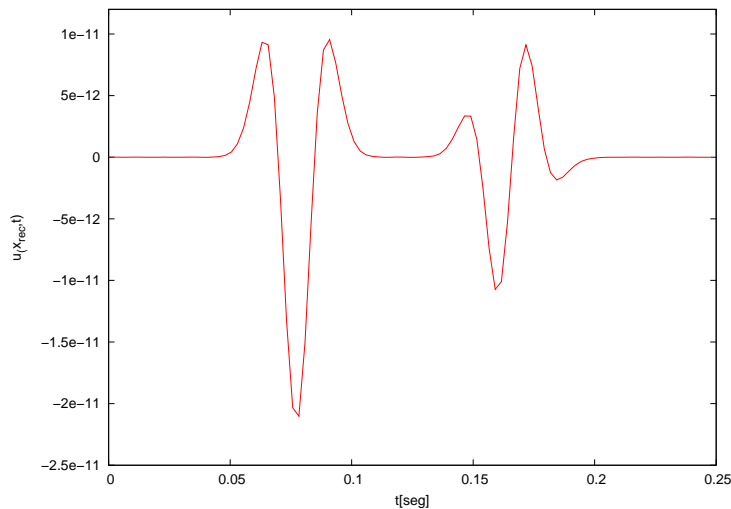

Figure 2: Seismic trace registered at location $x_{r1} = 850m$
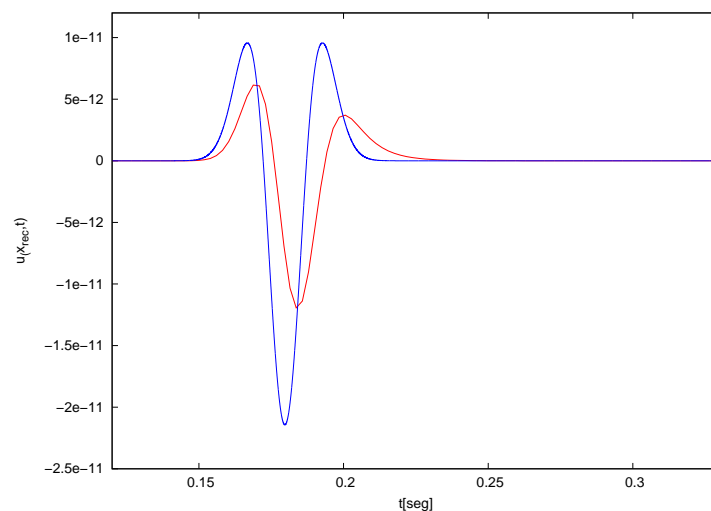

Figure 3: Seismic trace registered at location $x_{r2} = 1200m$. The central frequency of the source is $f_p = 30Hz$

In the first one we can observe, besides the direct arrival, a deformed wavelet that corresponds to the reflection wave generated in the fracture. The second trace shows another deformed wavelet, which corresponds to the transmission wave who passed through the fracture.

Van der Neut et al. (2008) developed a theoretical expression for the reflexion and transmission coefficients in a single fracture simulated using the linear slip model. This coefficients are frequency dependent, and the effects produced in the reflected and transmited waves are, for instance, phase time shifting and differential attenuation. The phase time shift effect can be seen in Fig. 2 because produces the wavelet deformation. To clearly observe the frequency dependent attenuation, Fig. 4 and Fig. 5 show the transmitted waves at position x_{r2} for sources with a central frequency of $15Hz$ and $45Hz$ respectively. We can see that for different central frequencies of the wavelet we have different attenuations.
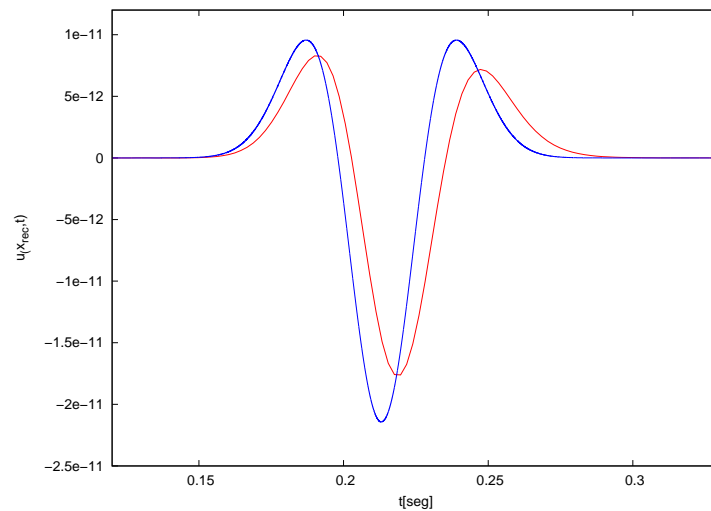

Figure 4: Seismic trace registered at location $x_{r2} = 1200m$. The central frequency of the source is $f_p = 15Hz$
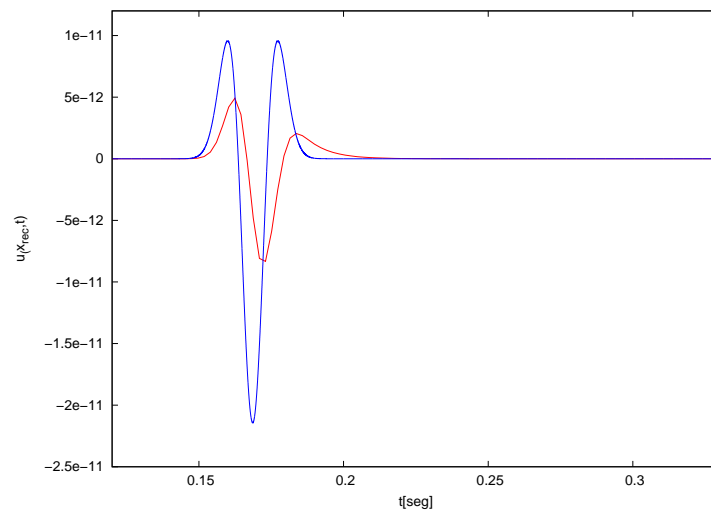

Figure 5: Seismic trace registered at location $x_{r2} = 1200m$. The central frequency of the source is $f_p = 45Hz$

5   CONCLUSIONS

In the present work, DGFEM were presented and implemented for solving the one-dimensional acoustic wave equation and a numerical simulator of wave propagation for elastic and hetero-

geneus media was generated. The DGFEM that presents the best results for the different sets of parameters considered is the Symmetric Interior Penalty Method (SIPG). The different methods present better stability for large enough values of penalty and the quadratic order is necessary for a good accuracy of the solution. The DGFEM allows us to easily and naturally implement in the numerical scheme the linear-slip model condition, and therefore to simulate the presence of a single fracture in the medium. The results obtained for such a medium are consistent with those obtained from previously published theoretical studies (Van der Neut et al., 2008). We observed that the presence of the fracture induces frequency dependent attenuation and phase time shifts in the reflexions and refractions of the impinging wave.

REFERENCES

Gauzellino P.M., Santos J.E., and Sheen D. Frequency domain wave propagation modelling in exploration seismology. *Journal of Computational Acoustics*, 9:941–955, 2001.

Golub G.H. and Van Loan C.H. *Matrix Computations, Third Edition*. John Hopkins University Press, USA, 1996.

Ricker N. The form and nature of seismic waves and the structure of seismograms. *Geophysics*, 5:348–366, 1940.

Riviere A. *Discontinuous Galerkin Methods for Solving Elliptic and Parabolic Equations: Theory and Implementation*. Frontiers in Applied Mathematics. SIAM, USA, 2008.

Schoenberg M. Elastic wave behavior across linear slip interfaces. *Journal of Acoustical Society of America*, 68:1516–1521, 1980.

Tassi P.A. and Vionnet C.A. Discontinuous galerkin method for the one dimensional simulation of shallow water flows. *Mecánica Computacional*, 22:1474–1488, 2003.

Udías A. *Principles of Seismology*. Cambridge University Press, 1999.

Van der Neut J., Sen M.K., and Wapenaar K. Seismic reflection coefficients of faults at low frequencies: a model study. *Geophysical Prospecting*, 56:287–292, 2008.

Álvarez Tagliabue C.U. and Marino P. Utilización del método de elementos finitos discontinuos para la resolución de la ecuación de transferencia radiativa. *Mecánica Computacional*, 26:3493–3511, 2007.

APPENDIX A

About the global matrix assemble

Due to the local support of the global basis functions, the linear system $A\vec{\alpha} = \vec{b}$ can be assembled from local linear systems derived in each element of the domain. From eq. (15) matrices E_n and D_n for $n = 1, 2, \cdots, N-1, n \neq \gamma$, are obtained by the interaction of the local basis functions between adjacent elements and have the form

$$
D_n = \begin{pmatrix}
-\dfrac{\sigma_n}{h_n} & -\dfrac{k_n}{h_n} + \dfrac{\sigma_n}{h_n} & 2\dfrac{k_n}{h_n} - \dfrac{\sigma_n}{h_n} \\[2ex]
-\epsilon\dfrac{k_{n-1}}{h_{n-1}} - \dfrac{\sigma_n}{h_n} & -\dfrac{k_n}{h_n} + \epsilon\dfrac{k_{n-1}}{h_{n-1}} + \dfrac{\sigma_n}{h_n} & 2\dfrac{k_n}{h_n} - \epsilon\dfrac{k_{n-1}}{h_{n-1}} - \dfrac{\sigma_n}{h_n} \\[2ex]
-2\epsilon\dfrac{k_{n-1}}{h_{n-1}} - \dfrac{\sigma_n}{h_n} & -\dfrac{k_n}{h_n} + 2\epsilon\dfrac{k_{n-1}}{h_{n-1}} + \dfrac{\sigma_n}{h_n} & 2\dfrac{k_n}{h_n} - 2\epsilon\dfrac{k_{n-1}}{h_{n-1}} - \dfrac{\sigma_n}{h_n}
\end{pmatrix},
$$

$$
E_n = \begin{pmatrix}
-\dfrac{\sigma_n}{h_n} & \dfrac{k_{n-1}}{h_{n-1}} - \dfrac{\sigma_n}{h_n} & 2\dfrac{k_{n-1}}{h_{n-1}} - \dfrac{\sigma_n}{h_n} \\[2ex]
\epsilon\dfrac{k_n}{h_n} + \dfrac{\sigma_n}{h_n} & -\dfrac{k_{n-1}}{h_{n-1}} + \epsilon\dfrac{k_n}{h_n} + \dfrac{\sigma_n}{h_n} & -2\dfrac{k_{n-1}}{h_{n-1}} + \epsilon\dfrac{k_n}{h_n} + \dfrac{\sigma_n}{h_n} \\[2ex]
-2\epsilon\dfrac{k_n}{h_n} - \dfrac{\sigma_n}{h_n} & \dfrac{k_{n-1}}{h_{n-1}} - 2\epsilon\dfrac{k_n}{h_n} - \dfrac{\sigma_n}{h_n} & 2\dfrac{k_{n-1}}{h_{n-1}} - 2\epsilon\dfrac{k_n}{h_n} - \dfrac{\sigma_n}{h_n}
\end{pmatrix} ;
$$

where k_n is the constant value of the longitudinal modulus k in the n-th element. The matrices M_n for $n = 0, 1, \cdots, N-1$, are given by

$$
M_0 = A_0 + F_0 + C_1;
$$
$$
M_n = A_n + B_n + C_{n+1}, \quad \forall n = 1, 2, \cdots, N-2;
$$
$$
M_{N-1} = A_{N-1} + B_{N-1} + F_N;
$$

where A_n for $n = 0, 1, \cdots, N-1$, are local matrices obtained from the integrals over the interval I_n and are as follows

$$
A_n = \begin{pmatrix}
-\omega^2 \rho_n h_n & 0 & -\dfrac{1}{3}\omega^2 \rho_n h_n \\[2ex]
0 & 4\dfrac{k_n}{h_n} - \dfrac{1}{3}\omega^2 \rho_n h_n & 0 \\[2ex]
-\dfrac{1}{3}\omega^2 \rho_n h_n & 0 & \dfrac{16}{3}\dfrac{k_n}{h_n} - \dfrac{1}{5}\omega^2 \rho_n h_n
\end{pmatrix} ,
$$

where ρ_n is the constant value of the density ρ in the element I_n; the local matrices B_n and C_n for $n = 1, 2, \cdots, N-1$, $n \neq \gamma$, are obtained from the interactions of the local basis functions with themselves in the elements I_n and I_{n-1} respectively, and have the form

$$
B_n = \begin{pmatrix}
\dfrac{\sigma_n}{h_n} & \dfrac{k_n}{h_n} - \dfrac{\sigma_n}{h_n} & -2\dfrac{k_n}{h_n} + \dfrac{\sigma_n}{h_n} \\[2ex]
-\epsilon\dfrac{k_n}{h_n} - \dfrac{\sigma_n}{h_n} & -\dfrac{k_n}{h_n} + \epsilon\dfrac{k_n}{h_n} + \dfrac{\sigma_n}{h_n} & 2\dfrac{k_n}{h_n} - \epsilon\dfrac{k_n}{h_n} - \dfrac{\sigma_n}{h_n} \\[2ex]
2\epsilon\dfrac{k_n}{h_n} + \dfrac{\sigma_n}{h_n} & \dfrac{k_n}{h_n} - 2\epsilon\dfrac{k_n}{h_n} - \dfrac{\sigma_n}{h_n} & -2\dfrac{k_n}{h_n} + 2\epsilon\dfrac{k_n}{h_n} + \dfrac{\sigma_n}{h_n}
\end{pmatrix} ,
$$

$$
C_n = \begin{pmatrix}
\dfrac{\sigma_n}{h_n} & -\dfrac{k_{n-1}}{h_{n-1}} + \dfrac{\sigma_n}{h_n} & -2\dfrac{k_{n-1}}{h_{n-1}} + \dfrac{\sigma_n}{h_n} \\[2ex]
\epsilon\dfrac{k_{n-1}}{h_{n-1}} + \dfrac{\sigma_n}{h_n} & -\dfrac{k_{n-1}}{h_{n-1}} + \epsilon\dfrac{k_{n-1}}{h_{n-1}} + \dfrac{\sigma_n}{h_n} & -2\dfrac{k_{n-1}}{h_{n-1}} + \epsilon\dfrac{k_{n-1}}{h_{n-1}} + \dfrac{\sigma_n}{h_n} \\[2ex]
2\epsilon\dfrac{k_{n-1}}{h_{n-1}} + \dfrac{\sigma_n}{h_n} & -\dfrac{k_{n-1}}{h_{n-1}} + 2\epsilon\dfrac{k_{n-1}}{h_{n-1}} + \dfrac{\sigma_n}{h_n} & -2\dfrac{k_{n-1}}{h_{n-1}} + 2\epsilon\dfrac{k_{n-1}}{h_{n-1}} + \dfrac{\sigma_n}{h_n}
\end{pmatrix} ;
$$

and the local matrices F_0 and F_N are obtained from the boundary conditions and are given by

$$F_0 = i\omega \left(k(x_0)\rho(x_0) \right)^{\frac{1}{2}} \begin{pmatrix} 1 & -1 & 1 \\ -1 & 1 & -1 \\ 1 & -1 & 1 \end{pmatrix},$$

$$F_N = i\omega \left(k(x_N)\rho(x_N) \right)^{\frac{1}{2}} \begin{pmatrix} 1 & 1 & 1 \\ 1 & 1 & 1 \\ 1 & 1 & 1 \end{pmatrix}.$$

The local matrices B_γ, C_γ, D_γ and E_γ for the element where the fracture is located are as follows

$$B_\gamma = \frac{1}{Z} \begin{pmatrix} 1 & -1 & 1 \\ -1 & 1 & -1 \\ 1 & -1 & 1 \end{pmatrix}, \qquad C_\gamma = \frac{1}{Z} \begin{pmatrix} 1 & 1 & 1 \\ 1 & 1 & 1 \\ 1 & 1 & 1 \end{pmatrix},$$

$$D_\gamma = \frac{1}{Z} \begin{pmatrix} -1 & 1 & -1 \\ -1 & 1 & -1 \\ -1 & 1 & -1 \end{pmatrix}, \qquad E_\gamma = \frac{1}{Z} \begin{pmatrix} -1 & -1 & -1 \\ 1 & 1 & 1 \\ -1 & -1 & -1 \end{pmatrix}.$$

About the explicit form of the right-hand side

Considering the point source defined in eq. (16), the coefficients b_i^n for $n = 0, 1 \cdots, N - 1$ and $i = 0, 1, 2$ are

$$b_i^n = \int_{x_0}^{x_N} \Phi_i^n(x)\delta'(x - x_f)\hat{f}_R(\omega)dx.$$

Because of the local support of the global basis functions and the well known properties of $\delta(x)$ the only nonzero coefficients are b_1^{nf} and b_2^{nf}, where nf is the element where the source is located. The explicit expressions for this coefficients for an uniform mesh are

$$b_1^{n_f} = -\frac{2}{h}\hat{f}_R(\omega),$$
$$b_2^{n_f} = -\frac{8}{h^2}\left(x_f - x_{n_f} - \frac{h}{2} \right)\hat{f}_R(\omega).$$

APPENDIX B

About the block tridiagonal LU factorization method

The Block Tridiagonal LU Factorization Method is a method for solving linear systems in which block tridiagonal matrices are involved. Due to the structure of this kind of matrices, this

method is better suited than, for instance, a band Gaussian elimination method (Golub and Van Loan, 1996).

To solve the system $A\vec{\alpha} = \vec{b}$ we start by considering a block LU factorization of the global matrix A in the form

$$
A = \begin{pmatrix}
I & 0 & \cdots & & 0 \\
L_1 & I & \ddots & & \vdots \\
0 & L_2 & \ddots & & \\
\vdots & \ddots & \ddots & I & 0 \\
0 & \cdots & 0 & L_{N-1} & I
\end{pmatrix}
\begin{pmatrix}
U_0 & D_1 & 0 & \cdots & 0 \\
0 & U_1 & D_2 & \ddots & \vdots \\
\vdots & \ddots & \ddots & \ddots & 0 \\
& & & U_{N-2} & D_{N-1} \\
0 & \cdots & & 0 & U_{N-1}
\end{pmatrix},
$$

where I is the 3×3 identity matrix and matrices U_0, L_i and U_i, $i = 1, 2, \cdots, N-1$ are obtained following the next procedure:

1. $U_0 = M_0$,

2. $i = 1$,

3. solve $L_i U_{i-1} = E_i$ for L_i,

4. $U_i = M_i - L_i D_i$,

5. $i = i + 1$; if $i < N$ go back to step 3, if $i = N$ stop.

Once A is factorized, $\vec{\alpha}$ can be obtained via block forward and back substitution:

1. $\vec{y}^{\,0} = \vec{b}^{\,0}$,

2. $i = 1$,

3. solve $\vec{y}^{\,i} = \vec{b}^{\,i} - L_i \vec{y}^{\,i-1}$,

4. $i = i + 1$; if $i < N$ go back to step 3, if $i = N$ continue to step 5,

5. solve $U_{N-1} \vec{\alpha}^{N-1} = \vec{y}^{\,N-1}$ for $\vec{\alpha}^{N-1}$,

6. $i = i - 1$,

7. solve $U_{i-1} \vec{\alpha}^{i-1} = \vec{y}^{\,i-1} - D_i \vec{\alpha}^{i}$ for $\vec{\alpha}^{i-1}$,

8. if $i > 0$ go back to step 6, if $i = 0$ stop.